Sea State Assimilation

Peter A.E.M. Janssen, Saleh Abdalla, Jean-Raymond Bidlot and Hans Hersbach

ECMWF
Shinfield Park
Reading, U.K.
p.janssen@ecmwf.int

ABSTRACT

The prospect of global observations of surface winds and waves gave a significant stimulus to wave model development in the 1980's, while the need to have reliable wave predictions stimulated the development of remote sensing instruments that could provide accurate wind and wave products on a global scale. We discuss in this paper the use of satellite observations in the ECMWF wave forecasting system.

1 Introduction

Before we discuss the subject of assimilation of satellite observations in an ocean-wave forecasting system, first a brief introduction into the field of surface gravity waves and ocean wave forecasting is given.

The programme of this paper is therefore as follows. Wave forecasting is based on a spectral description of the sea state. The basic evolution equation of the wave spectrum is the *energy balance equation* A number of applications, in deterministic and ensemble prediction will be discussed. Next, we describe the main topic of this paper, namely the assimilation of altimeter wave height and Synthetic Aperture Radar (SAR) spectra. For each instrument we discuss the observation principle, the analysis method and the impact on wave analysis and forecast. Although altimeter wind speed data are not used in the analysis, they are extremely useful for validation purposes because they are really *independent*. Finally, scatterometer winds obey the same observation principle as the SAR, and these wind vector observations are of great value in specifying the driving surface winds. As an illustration we discuss the recent operational introduction of ASCAT wind observations from Metop A.

2 Wave theory

In Fig. 1 a schematic of the problem is given and some relevant quantities are introduced. Ocean waves are surface gravity waves that obey the dispersion relation $\omega = (g|\mathbf{k}|)^{1/2}$. They are generated by the surface wind and they grow until limited by dissipation due to white-capping (see Fig. 2) or by four-wave interactions. Once ocean waves leave the storm area they are not subject to wind forcing anymore and are only subject to white-cap dissipation. The steep waves (called wind sea) turn into gentle swells which may propagate over large distances across the oceans.

There are a number of reasons why forecasting of individual ocean waves is not possible, hence we consider the evolution of the average seastate: a spectral description!
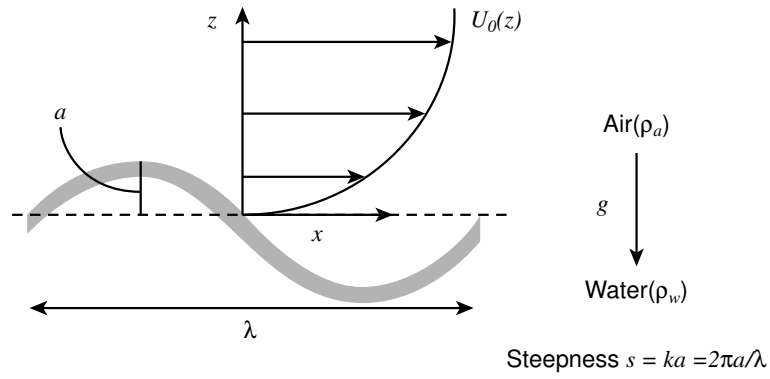
Figure 1: Schematic of the problem in two dimensions.

Figure 2: Ilustration of how complicated the sea state looks like for a wind speed of 18 m/s.

2.1 Energy balance equation

Therefore concentrate on the prediction of the ensemble average of the action density spectrum $N(\mathbf{k};\mathbf{x},t)$. Action plays the role of a number density and is defined in such a way that energy spectrum $F(\mathbf{k};\mathbf{x},t)$ is given as

$$F(\mathbf{k};\mathbf{x},t) = \omega(\mathbf{k}) \times N(\mathbf{k};\mathbf{x},t)$$

which is the usual rule in wave mechanics. From first principles one finds the following evolution equation (Komen *et al.*, 1994; Janssen, 2004)

$$\frac{\partial}{\partial t}N + \nabla_{\mathbf{x}} \cdot (\dot{\mathbf{x}}N) + \nabla_{\mathbf{k}} \cdot (\dot{\mathbf{k}}N) = S = S_{in} + S_{nl} + S_{ds},$$

where $\dot{\mathbf{x}} = \partial\omega/\partial\mathbf{k}$, $\dot{\mathbf{k}} = -\partial\omega/\partial\mathbf{x}$, and the source functions S represent the physics of wind-wave generation, dissipation by wave breaking and nonlinear four-wave interactions. Once the evolution of the wave spectrum is known, parameters such as significant wave height H_S follow by instegration of the wave spectrum over wavenumber space. For example

$$H_S = 4\sqrt{E}, \; E = \int d\mathbf{k}\, F(\mathbf{k};\mathbf{x},t).$$

2.2 Wave forecasting

The energy balance equation (including nonlinear transfer) is solved by modern wave prediction systems, where the forcing of the waves is provided by surface winds from weather prediction systems. From experience it is known that a large part ($\pm 80\%$) of the quality of the wave forecast is determined by the accuracy of the surface wind field.

In Fig. 3 we show the time evolution of the frequency spectrum for an infinite ocean and a wind speed of 18.5 m/s, while the right panel shows the energy balance, i.e. the source functions as function of frequency after a duration of 3 hrs.
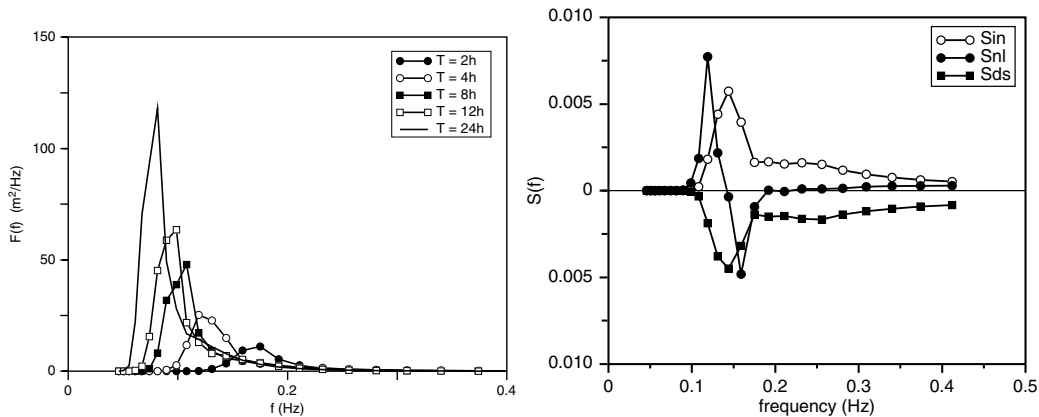

Figure 3: Evolution in time of the one-dimensional frequency spectrum for a wind speed (left) and the right panel shows the energy balance after a duration of 3 hrs.
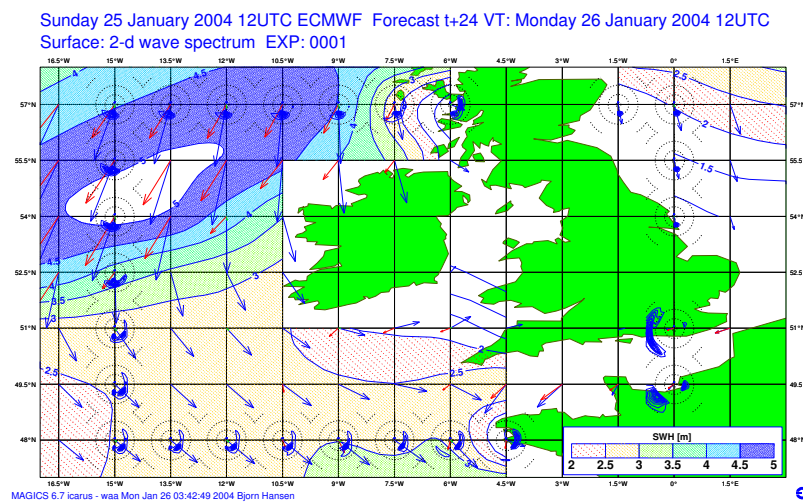

Figure 4: Boundary conditions for the Irish Met Office model.

Ocean wave forecasting at ECMWF is based on WAM cy4 (Janssen, 2004). Discuss global implementation only. Presently, the global version of the wave model covers the region from 81° S to 81° N. It is coupled to the atmospheric model (two-way interaction with feedback of ocean waves on ocean surface roughness) since June 29, 1998 thus giving a sea-state dependent momentum and heat flux. Two types of forecasts are provided: Deterministic and probablistic forecasts.

For deterministic forecasts the wave spectrum $F(f, \theta)$ has 30 frequencies and 24 directions. The wave model

is coupled to the 10 m winds from T_l799 IFS model every timestep Δt of 12 min. The model runs on an irregular lat-lon grid, $\Delta x = 40$ km, and the initial condition of the wave forecast is prepared by assimilation of ENVISAT & Jason altimeter H_S and ENVISAT ASAR spectra. Every day 10 day forecasts from 00Z and 12 Z are produced. An example of daily output, in this case spectral data for Met Eiran's limited area wave model, is shown in Fig. 4.
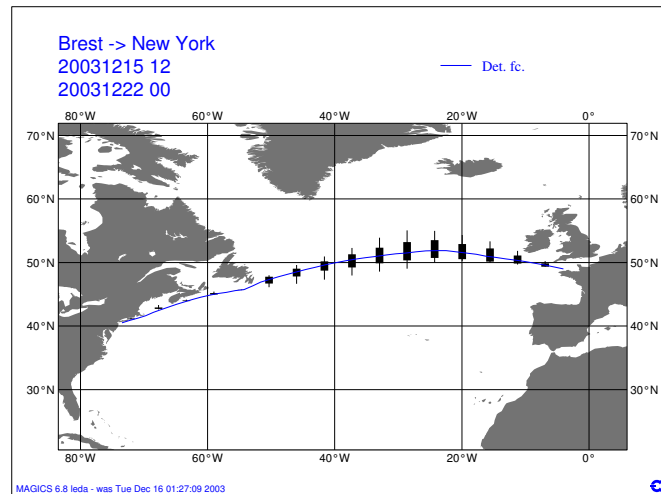

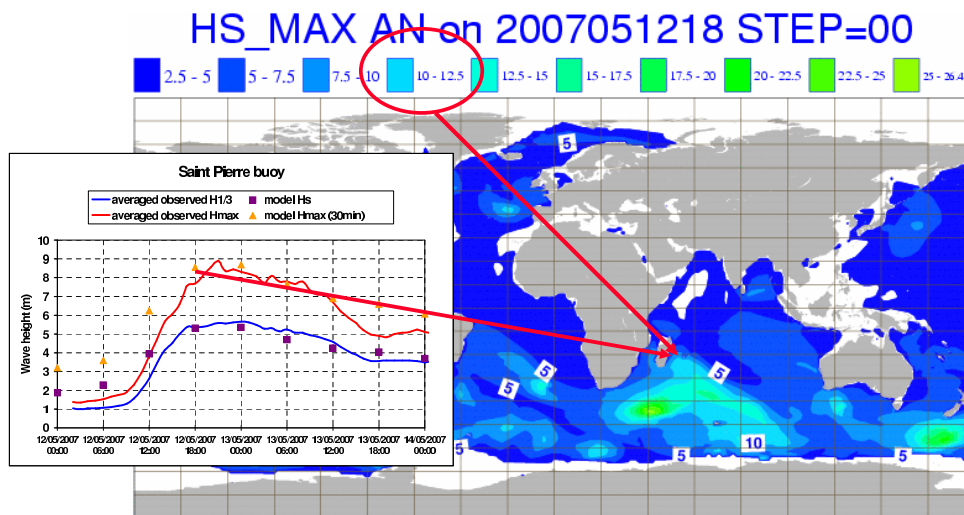*Figure 5: Uncertainty in predicted ship route as follows from the EPS.*

Figure 6: Extreme wave heights near La Réunion on May 12 2007.

In addition, in order to have an a priori estimate of forecast uncertainty, probabilistic forecasts of the sea state are made as well. This is relatively straightforward as the EPS is run in two-way interaction mode. Hence one control forecast and a 50-member ensemble is produced with a version of the coupled IFS-wave model that has about half the spatial resolution of the deterministic system. As an illustration of the potential use of probablistic forecasting we mention that presently maps showing the probability of high sea states are produced. Also, ship routing is an important application. The error in forecast ship route may be obtained from the 50 ship routes generated by the winds and waves of the 50-member ensemble, as illustrated in Fig. 5.

2.3 Maximum wave height

Although wave forecasting is about the mean sea state in a grid box one can also make statements about deviations from the mean, as expressed by the maximum wave height during a given time period. An example is the recent extreme event at La Réunion, which is displayed in Fig. 6 This product, which is based on the known probability distribution function of the surface elevation, will become available in early 2008.

3 Altimeter data

3.1 Measurement principle

The altimeter is a radar (usually operating at Ku-band) that transmits a pulse towards the sea surface at nadir. *Significant wave height H_S* is then determined from the slope of the return pulse (the wave form), while *wind speed* follows from the total backscatter.

For a random sea the return pulse also depends on the probability distribution of the ocean waves. In good approximation this is a Gaussian, but nonlinear effects, giving sharper crests and wider throughs, result in a skewed distribution. As a consequence, the waveform is retarded, as illustrated in the next figure, and therefore an altimeter measures a slightly longer range (of the order of $5\%H_S$) than the actual distance between satellite and mean ocean surface. The difference between the two is called the *sea-state bias* and is directly related to properties of ocean waves such as the mean square slope and wave age (Kumar et al, 2003).
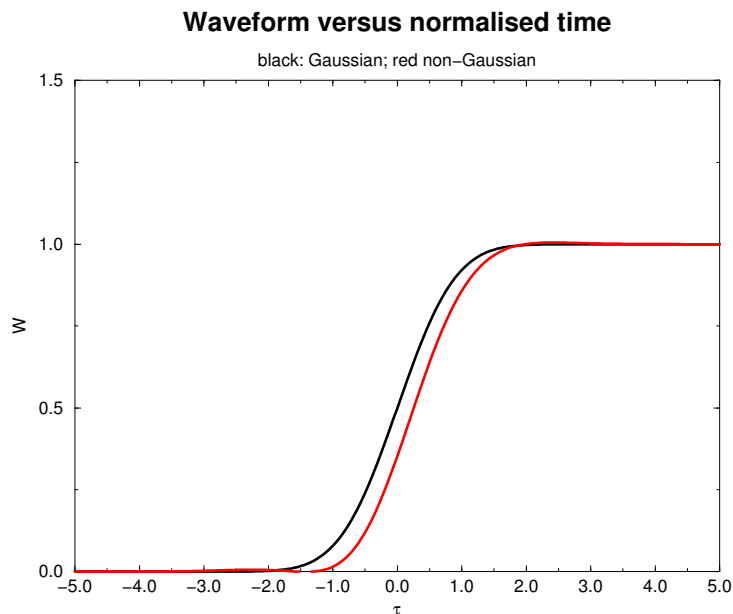

Waveform versus normalised time

Figure 7: Theoretical wave form for a flat sea surface. Effects of skewness on the wave form are shown as well.

3.2 Analysis method

Two problems in wave height analysis:

- The wave spectrum has 30×24 degrees of freedom while we only provide observed information on an integral of the wave spectrum $\Rightarrow$ *too many degrees of freedom*!

- Windsea is *strongly coupled* to the generating winds, hence a change in wave height implies, to be consistent, a change in local wind.

The many degrees of freedom problem is solved by using our knowledge on the evolution of ocean waves. Analysed spectrum is obtained by scaling the first-guess spectrum, where the scaling constants A and B depend on first-guess and observed parameters

$$F_{an}(f,\theta) = AF_{fg}(Bf, \theta + \Delta\theta),$$

where F_{fg} is rotated by an amount $\Delta\theta$ if this information is available (e.g. from a SAR). The scaling constants A and B follow from the dynamics of waves.

Consider the example of *windsea*. JONSWAP(1973) has shown that the windsea spectrum has a universal shape depending on a single parameter, the wave age χ,

$$\chi = \frac{c_p}{u_*}, \ c_p = \frac{g}{\omega_p},$$

where ω_p is the peak frequency of the windsea. Hence the dimensionless energy $\varepsilon_* = g^2 E / u_*^4$ follows from the scaling law

$$\varepsilon_* = const \ \chi^3.$$

A simple analysis scheme can then be build by making the basic assumption that the first-guess wave age χ_{fg} is correct!

Then, from analysed H_S (using Optimum Interpolation) and first-guess H_S the analysed friction velocity $u_{*,an}$ becomes

$$u_{*,an} = u_{*,fg} \sqrt{\frac{H_{S,an}}{H_{S,fg}}},$$

while the peak frequency $f_{p,an}$ follows from $\chi_{an} = \chi_{fg}$. Finally, the two scaling parameters of the spectrum follow from the requirement that analysed spectrum gives the analysed wave height, hence,

$$A = \left(\frac{H_{S,an}}{H_{S,fg}}\right)^2 B, \ B = \frac{f_{p,an}}{f_{p,fg}}$$

In a comprehensive wind and wave assimilation system, corrected winds would go into the atmospheric assimilation scheme to provide an improved wind field in the forecast. This approach has not been pursued yet.
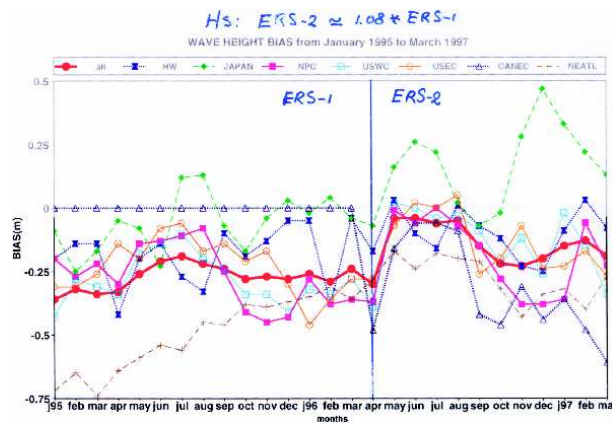

Figure 8: Importance of quality altimeter data as follows from validation of the analysis against buoy data. The switch from ERs-1 to ERS-2 data occurred on April 30 1996.
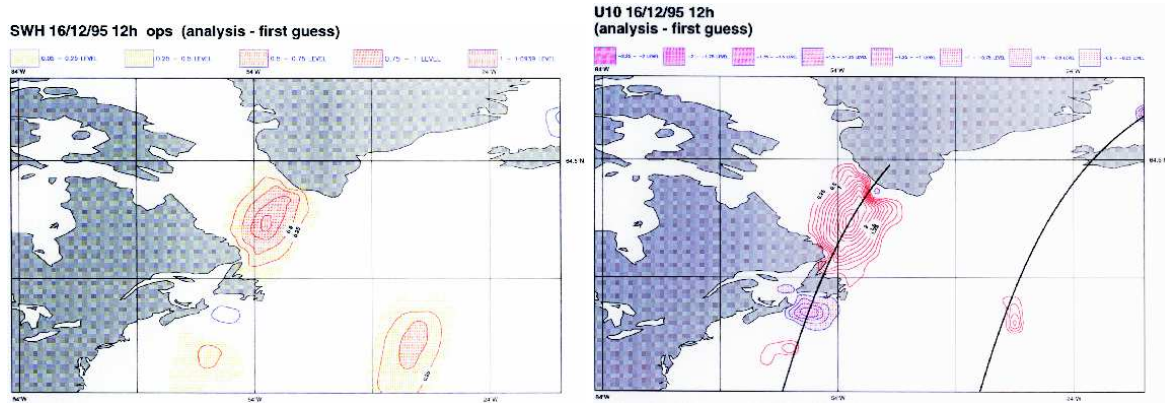
Figure 9: Wave height increments(left and corresponding wind speed increments.
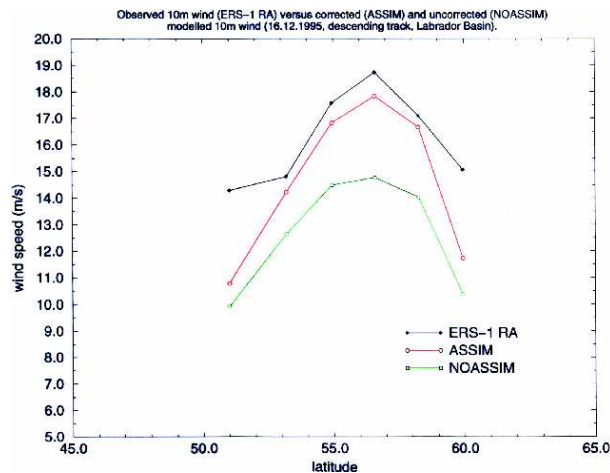

Figure 10: Validation of analyzed wind against altimeter winds.

3.3 Results

Optimum Interpolation schemes of the type just described have been operational since mid 1993 at UKMO (until beginning 2000) and ECMWF (while at NCEP from 1998 until February 2000). More recently also at Meteo-France and BoM.

Results at ECMWF show that the impact of altimeter data on wave analysis and forecast is positive. However, all this relies on the quality of the observations from the ESA altimeters. For example, the ERS-2 altimeter produced, when compared to buoy data, much better estimates of significant wave height than its predecessor ERS-1. This was immediately evident when the ERS-2 altimeter was introduced on April 30 1996 (and the ERS-1 assimilation was switched off) as the analyzed wave height bias (compared to Buoy data) reduced considerably (see Fig. 8). Impact on the quality of wave height fields from the Reanalysis.

In the Figs. 9-10 we show by way of an example that the wind-wave analysis scheme works well, producing when compared to the altimeter winds, reasonable estimates of wind speed.

3.4 Impact on forecast

- Altimeter wave height data have a limited impact on *global* forecast skill, but in areas where *swell* is important, impact on forecast is more substantial. This is shown in Fig. 11 over a three month period in the winter of 2006-2007 by verifying forecasts against ENVISAT altimeter wave height data.
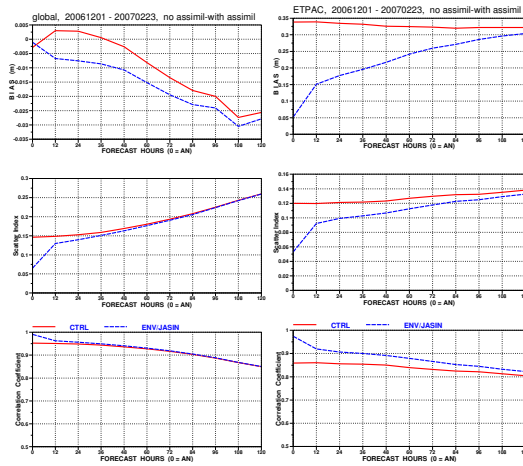
Figure 11: Impact of ERS-2 altimeter wave height data assimilation on ECMWF wave height forecast obtained by comparing wave height forecast against ENVISAT wave height observations. Period is about three months in the winter of 2006-2007. Left panels for the global area and right panels for the eastern Pacific.
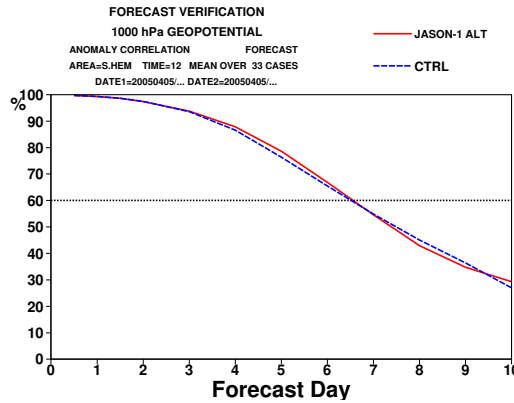

Figure 12: Impact of the introduction of the assimilation of Jasin-1 significant wave heights on the forecast skill of the 1000 mb geopotential height.

- However, occasionally there is a systematic impact also in windsea cases on atmospheric scores (see Fig. 12). Note that ECMWF runs a coupled weather, ocean wave model where the roughness over the oceans is sea state dependent.

4 Synthetic Aperture Radar data

4.1 Measurement principle

The Synthetic Aperture Radar (SAR) measures the modulation of short waves (observed by Bragg scattering) by long gravity waves, slicks, internal waves, currents, etc.

The SAR inversion scheme of Hasselmann and Hasselmann (1990) considers three types of *modulation*

- tilt modulation.

- hydrodynamic modulation (refraction caused by orbital motion of long waves).

- velocity bunching: phase information distorted by long wave orbital motion.

As a consequence, the *SAR image spectrum* is a nonlinear function of the wave spectrum. Inversion requires a reliable, accurate first-guess spectrum. The MPI inversion algorithm, operational at ECMWF uses as first-guess the appropriate model wave spectrum.

Velocity bunching

A SAR scans the modulated backscatter field $I_R(\mathbf{x},t)$ in the range (across-track) direction and achieves spatial resolution of the order of 10 m, but in the azimuth (along-track) direction resolution is poor. In order to improve on this (see Fig. 13 for an explanation of symbols) the SAR uses phase information to locate the azimuthal position of the backscattering element: the facet is located at *zero Doppler shift*. This localization in azimuth
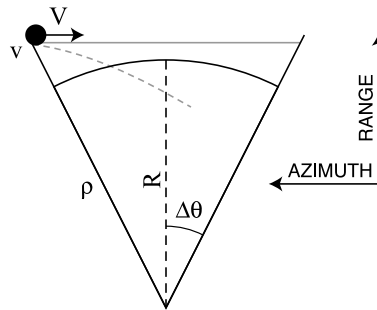

Figure 13: Definition sketch of the velocity bunching problem with a SAR.

works very well for stationary objects, but when an facet resides on a moving surface with range component of the orbital velocity v, then there is an additional Doppler shift, and hence the SAR positions the object in the wrong location. The corresponding azimuthal displacement $\xi(\mathbf{x})$ at a location $\mathbf{x}$ is then given by

$$\xi(\mathbf{x}) = \beta v, \ \beta = R/V = \mathcal{O}(100)$$

Because β is large this results in displacements of the order of 200 m.

The velocity bunching effect leads to considerable distortions of the actual surface wave spectrum $F(\mathbf{k})$. As a consequence, short waves (in practice with a wavelength less than 200 m) are not properly represented by a SAR. In the so-called quasi-linear approximation one finds for the SAR spectrum $F_{SAR}(\mathbf{k})$,

$$F_{SAR}(\mathbf{k}) = \exp(-\beta^2 \langle v^2 \rangle k_y^2) \times F(\mathbf{k}),$$

where k_y is the wavenumber in the azimuth direction. The resulting distortion of the wave spectrum and the sea surface elevation is displayed in Fig. 14
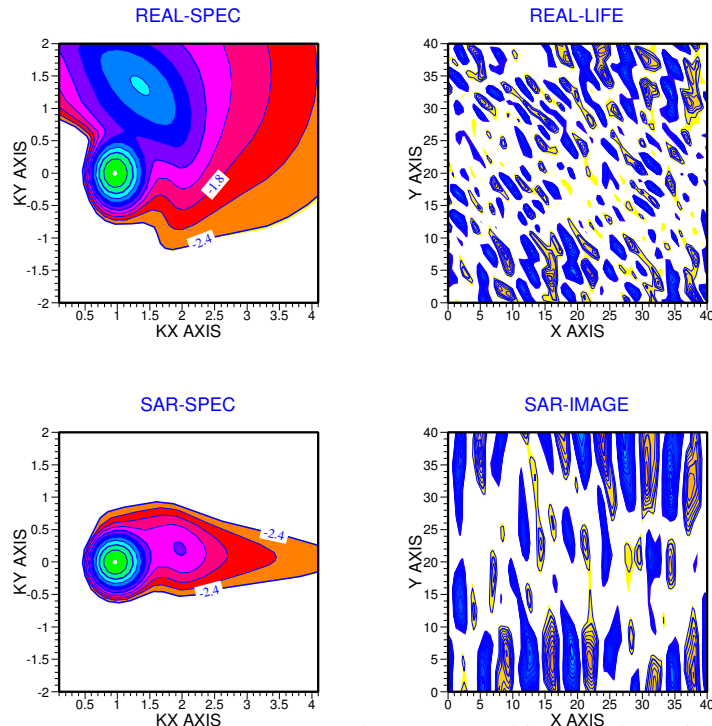
Figure 14: Distortion of the sea surface elevation signal by the velocity bunching effect.

4.2 Analysis method

Assume that we have given a SAR spectrum which is obtained from the SAR image spectrum using the first-guess WAM model spectrum.

The method to assimilate SAR data proceeds as follows:

- Identify a number of *dominant wave systems* in the SAR spectrum and in first-guess and label these by means of energy, mean direction and peak frequency.

- Apply the *scaling laws*

$$F_{an}(f, \theta) = AF_{fg}(Bf, \theta + \Delta\theta),$$

  with $B = f_{p,an}/f_{p,fg}$ and $A = BE_{an}/E_{fg}$ but now to each wave system.

- For the *windsea system* infer analysed wind speed by means of scaling law between energy and wave age.

4.3 Results

According to the literature impact of SAR data on analysis is relatively small. After a lot of work Jean Bidlot found a somewhat larger impact.

One reason for the small impact on wave height is probably the relative abundance of altimeter wave height data. Also, results depend on how in the inversion scheme the SAR data are *calibrated*. Comparison of SAR and buoy spectra (Voorrips et al, 2001) suggests that this calibration has not always been optimal in the past.

To illustrate the impact of SAR data we quote in Table 1 statistics from an experiment for February 1998, where all results are compared with buoy data. Note that more recent experiments have shown a less favourable impact for SAR data.

EXP	rms (m)	Bias (m)	SI(%)
REF	0.583	-0.285	0.167
SAR	0.531	-0.224	0.158
ALT	0.537	-0.191	0.165
ALT+SAR	0.510	-0.177	0.157

Table 1: Scores for H_S ($N = 5560$) for February 1998. REF is the reference run (a hindcast), SAR means only SAR assimilation, ALT means only altimeter assimilation and ALT+SAR means assimilating both data.

The Figs. 15-16 show an example of an inversion, and a comparison of analysis increments from SAR and altimeter assimilation.
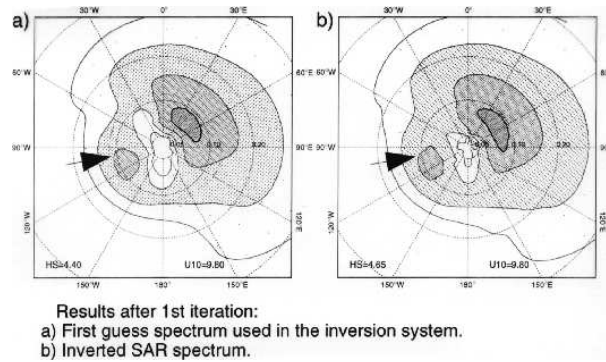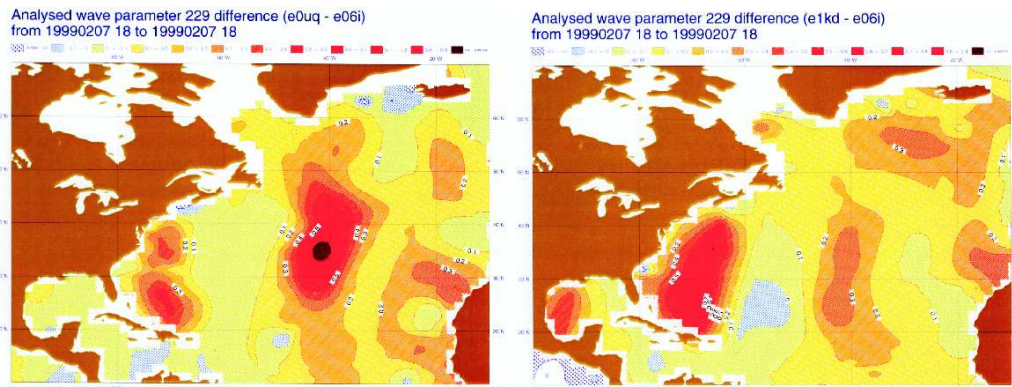

Figure 15: Example of a SAR inversion.

Figure 16: Analysis increments due to SAR data (left) and due to altimeter data.

5   Altimeter wind speed data

According to altimeter measurement theory the total radar return (called the backscatter σ_0) is inversely proportional to the mean square slope of the sea surface s^2. In fact,

$$\sigma_0 = \frac{|R(0)|^2}{s^2},$$

where $R(0)$ is a reflection coefficient. The mean square slope is mainly determined by the short waves which are the waves that are under direct influence of the wind. Consequently, there is a strong correlation between σ_0 and the surface wind. Before this will be discussed in more detail at the end of this section we first discuss the value of the altimeter wind speed data as a monitoring tool.

Altimeter wind speed data are not assimilated in the ECMWF atmospheric model, but, rather, these (independent) data are used to *monitor* the quality of the modelled surface wind speeds. This is illustrated by a comparison of analyzed and altimeter wind speed over a 5 year period in Fig. 17, illustrating the progress ECMWF has made in modelling the surface wind.
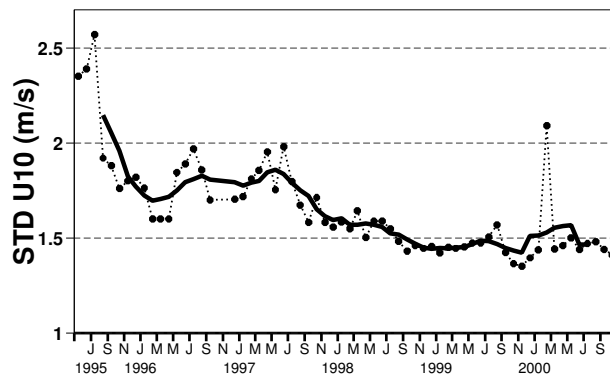

Figure 17: *Comparison of analyzed and altimeter wind speed over a 5 year period starting in May 1995. Note that in early 2000 the altimeter failed due to loss of its capability to maintain orientation.*

Nevertheless, there are problems for the low wind speed range. Abdalla (2007) found based on the assumption that σ_0 only depends on the surface wind speed U_{10} (hence no sea state effects) a very satisfactory solution. A fit was made using collocated model wind speed data and buoy winds over a two month period.
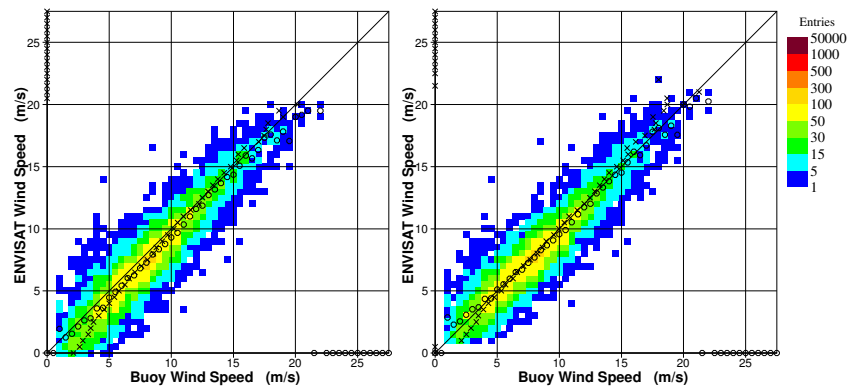

Figure 18: *Comparison of altimeter wind speed against buoy data using the MCW algorithm (left) and using Abdalla's approach (right).*

A validation of the Abdalla algorithm against buoy wind speed data and a similar comparison using the 'classical' MCW algorithm (Witter and Chelton, 1991) is shown in Fig. 18. It shows that to the Abdalla algorithm gives, when compared to the MCW algorithm, considerable improvements in the low wind speed range.

However, many researchers nowadays believe that the relation between radar backscatter and wind speed should also involve a measure of the sea state. Following this idea we have made our own 'physical' wind speed algorithm that starts from the theoretical relation between backscatter and mean square slope and uses the mean square slope s^2 from the wave model, which gives a fair representation of the sea state up to a cut-off wavenumber $k \simeq 1$. The high-wavenumber part of the spectrum is obtained from the VIERS model (Janssen *et*
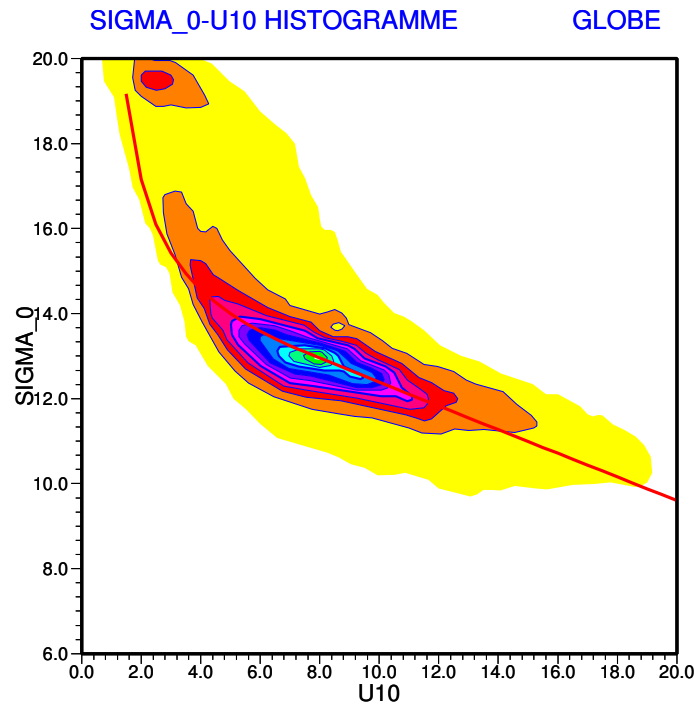
Figure 19: Two dimensional histogram showing the relation between radar backscatter σ_0 and surface wind speed U_{10} obtained from a model of radar backscatter based on specular reflection. Here the slope is obtained from the WAM-VIERS model. As a reference, the σ_0-U_{10} relation according to Abdalla is shown as the red line.

al., 1998) that includes the physics of wind input, nonlinear 3-wave interactions and dissipation).

As shown in Fig. 19, the 'physical' wind speed algorithm shows good agreement with the Abdalla fit (corrected by 2.24 dB to refer to absolute backscatter), therefore σ_0 depends on the sea state. However, since the mean square slope is largely determined by the high-wavenumber part of the spectrum, σ_0 highly correlates with the surface wind speed.

6 Scatterometer winds

Scatterometer winds follow from the same physical principle as the SAR images, i.e. Bragg scattering, but rather than looking at the modulations in the backscatter, one records the average backscatter over an area of say 25×25 km..

The ASCAT instrument is of similar design as the AMI scatterometers on board of ERS-1/2 from which data has been operationally assimilated at ECMWF since 30 January 1996. Triplets of radar backscatter from three antennas are combined to estimate surface vector winds over the global oceans. Both AMI and ASCAT operate at C-band (5.3 GHz) and have the same antenna geometry. Two main differences are a different range of incidence angle (optimized for ASCAT to enhance performance in wind direction) and the fact that ASCAT carries two sets of antennas (providing two swaths that double the coverage). ASCAT data has been monitored at ECMWF from the start of dissemination by EUMETSAT via the EUMet-Cast system on the 31th of January 2007. Surface winds are inverted from available (level 1b) backscatter triplets on the basis of a modified version of the geophysical model function CMOD5 (Hersbach *et al.*, 2007). Resulting winds are collocated with operational short-range ECMWF forecast winds. The monitoring confirms that the ASCAT instrument is working well.
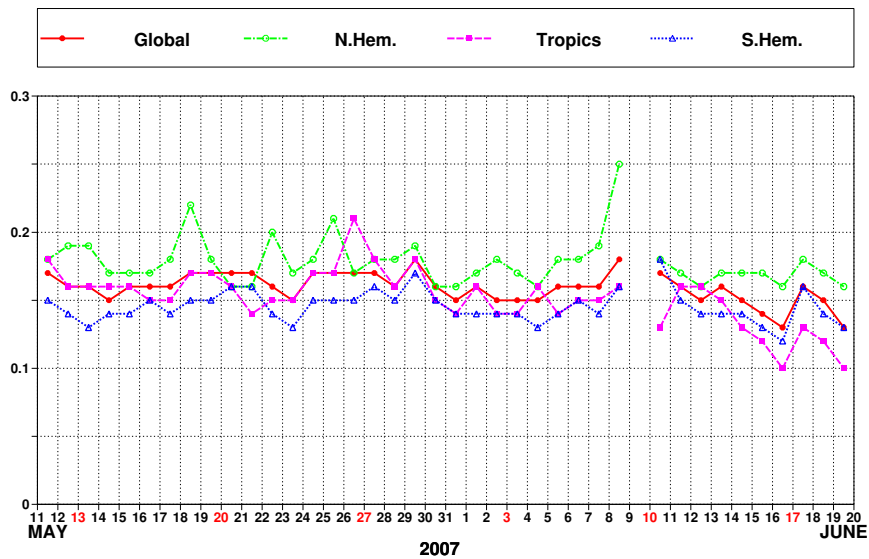
ENVISAT Radar Altimeter wind Wind Speeds: Timeseries of scatter Index (SI) (analysis)

Figure 20: Timeseries of scatter index (SI) of the difference between ENVISAT altimeter and analyzed ECMWF wind speed. Note that on the 12th of June 2007 the assimilation of ASCAT data was introduced in operations giving a closer match between altimeter and analyzed wind.

Assimilation experiments with the ASCAT data confirmed the high quality of the product as there were small but significant improvements in forecast performance, in particular in the Southern Hemisphere scores of 1000 and 500 hPa geopotential. On the 12th of June 2007 ECMWF was the first to present these data to the analysis scheme. Improvements of the analyzed surface winds were already evident after a few days as is shown in Fig. 20. Here, for different areas on the globe, timeseries of normalized standard deviation of error (SI) of the difference between ENVISAT altimeter wind speed and analyzed windspeed are shown for the period of the 11th of May until the 20th of June, 2007. The assimilation of ASCAT data commenced on the 12th of June and the impact of these new observations on the quality of the surface analysis is clearly visible after a few days.

7 Conclusions

We conclude the following:

- Altimeter wave height data and SAR spectral data are of high quality, producing an *accurate* surface wave analysis, while scatterometer data, in particular ASCAT data, have considerable value for the surface wind analysis (and even in the upper layers of the atmosphere).

- Altimeter wave height and wind speed data have tremendous value for *diagnosing* wave model problems and problems with the model surface winds

- Recently it was shown that using only wave model information a realistic representation of specular reflection from the ocean surface may be given. This implies that wave model information will be of value in specifying the *ocean surface albedo* and it will be of value in the interpretation of other satellite sensors such as scatterometer, ATOVS, SSM/I.

References

S. Abdalla, 2007. Ku-band radar altimeter surface wind speed algorithm. *ECMWF Technical Memorandum*, **524**.

K. Hasselmann, T.P. Barnett, E. Bouws, H. Carlson, D.E. Cartwright, K. Enke, J.A. Ewing, H. Gienapp, D.E. Hasselmann, P. Kruseman, A. Meerburg, P. Müller, D.J. Olbers, K. Richter, W. Sell, H. Walden, Measurements of wind-wave growth and swell decay during the Joint North Sea Wave Project (JONSWAP), Dtsch. Hydrogr. Z. Suppl. A 8(12) (1973) 95p.

K. Hasselmann, and S. Hasselmann, 1991. On the nonlinear mapping of an ocean wave spectrum into a SAR image spectrum and its inversion. *J. Geophys. Res.*, **C96**, 10713-10729.

H. Hersbach, A. Stoffelen, and S. de Haan, 2007. An improved C-band scatterometer ocean geophysical model function: CMOD5. *J. Geophys. Res.* **112** C03006.

P.A.E.M. Janssen, *The Interaction of Ocean Waves and Wind*, Cambridge University Press, Cambridge, U.K., 2004, 300+viii pp.

P.A.E.M Janssen, H. Wallbrink, C.J. Calkoen, D. van Halsema, W.A. Oost and P. Snoeij, 1998. VIERS-1 scatterometer model. *J. Geophys. Res.* **103** (No. C4), 7807-7831.

G.J. Komen, L. Cavaleri, M. Donelan, K. Hasselmann, S. Hasselmann, and P.A.E.M. Janssen, 1994: *Dynamics and Modelling of Ocean waves* (Cambridge University Press, Cambridge), 532 p.

R. Kumar, D. Stammer, W.K. Melville, P. Janssen, 2003. Electromagnetic bias estimates based on TOPEX, buoy, and wave model data. *J. Geophys. Research* **108**, 3351,doi:10.1029/2002JC001525.

A.C. Voorrips, C. Mastenbroek, and B. Hansen, 2001. Validation of two algorithms to retrieve ocean wave spectra from ERS synthetic aperture radar. *J. Geophys. Res.* **106**, No. C8, 16,825-16,840.

D.L. Witter and D.B. Chelton, 1991: A Geosat Altimeter Wind Speed Algorithm and a Method for Altimeter Wind Speed Algorithm Development. *J. Geophys. Res.* **96**, 8853-8860.